

Models for Evolution of Dusty Galaxies and E/S0s Seen in Multiband Surveys

C. K. Xu, C. J. Lonsdale, D. L. Shupe

Infrared Processing and Analysis Center, Jet Propulsion Laboratory, Caltech 100-22,
Pasadena, CA 91125, USA

A. Franceschini

Dipartimento di Astronomia, Universita' di Padova, Vicolo dell'Osservatorio 5, I-35122,
Padova, Italy

C. Martin, D. Schiminovich

California Institute of Technology, Pasadena, CA 91125, USA

Received 7.12.2002; accepted 12.13.2002

ABSTRACT

Phenomenological models for evolution of dusty galaxies and E/S0 galaxies, respectively, are developed to address two major questions concerning galaxy populations in deep infrared (IR) surveys: (1) Do normal late-type galaxies or starburst galaxies (including galaxies with obscured AGNs) dominate among sources in deep IR surveys? (2) How much do E/S0 galaxies contribute to the counts in deep mid-infrared (MIR: $3 - 20\mu m$) surveys? Among three new models for evolution of dusty galaxies, it is assumed in Model S1 that starburst galaxies are the dominant population, and in Model S2 that normal galaxies dominate. Model S3 is an intermediate model. Comparing the model predictions with a wide range of observational data collected from the literature, we find that none of these models can be ruled out, given the uncertainties of the data. We show that the most direct method to distinguish these models is to compare the predicted color distributions of IR galaxies with observations, which will soon be available from the SWIRE survey. The models for E/S0 galaxies follow a simple passive evolution approach. Among the three E/S0 models (E1, E2 and E3) investigated in this paper, Model E2 which is specified by a peak formation redshift $z_{peak} = 2$, and an e-folding formation time scale $\omega = 2$ Gyr, fits the data best. This suggests a synchronization between the evolution of E/S0 galaxies and of starburst galaxies, in the sense that the peak of the formation function of E/S0s ($z_{peak} = 2$) is close to the peak of the evolution functions of starburst galaxies ($z_{peak} = 1.4$). We find that E/S0s contribute about 10 – 30% of the counts in the MIR bands of $< 10\mu m$, and up to 30 – 50% of the optical/NIR counts in the bright end. Their contributions to counts in the UV (2000Å) and in the longer wavelength IR ($\geq 12\mu m$) bands are negligible. Taking into account this contribution, new predictions for counts and confusion limits in the SIRTf bands are presented.

Subject headings: galaxies: evolution – starburst – elliptical and lenticular –
Seyfert – luminosity function; infrared: galaxies

1. Introduction

Many new windows have recently been opened in various wavebands for observations of high redshift galaxies. Particularly, deep ISO surveys (e.g. Rowan-Robinson et al. 1997; Franceschini et al. 1997; Kawara et al. 1998; Elbaz et al. 1999; Aussel et al. 1999; Flores et al. 1999b; Puget et al. 1999; Dole et al. 2001; Clements et al. 1999; Serjeant et al. 2000) in the infrared and SCUBA surveys (Hughes et al. 1998; Barger et al. 1998; Blain et al. 1999) in the submm wavebands have shed lights on the dark side of galaxy formation and evolution. This stimulated a surging wave of empirical models (Xu et al. 1998; Blain et al. 1999; Roche & Eales 1999; Dole et al. 2001; Xu 2000; Rowan-Robinson 2001; Xu et al. 2001; Franceschini et al. 2001; Pearson 2001; Malkan & Stecker 2001; Chary & Elbaz 2001) to interpret the new ISO and SCUBA sources. The main aim of these empirical models is to better constrain some important characteristics of the galaxy evolution, including the peak epoch of the star formation rate in the universe and the roles played by different star formation modes (e.g. the quiescent mode against the interaction stimulated mode), for which the earlier optical deep surveys such as the Hubble Deep Field Survey (Williams et al. 1996) may have provided biased information (Madau et al. 1996) by neglecting the dust extinction (Rowan-Robinson et al. 1997; Lonsdale 1999). This will certainly have impact on the theoretical simulations of galaxy formation and evolution, which (e.g. Somerville et al. 2001) have just started facing the fact that most of the early star formation may be hidden behind a thick veil of dust, making the incorporation of effects of dust extinction and emission in the framework essential (Granato et al. 2000).

Some of the most recent empirical models (Rowan-Robinson 2001; Xu et al. 2001;

Franceschini et al. 2001; Pearson 2001; Chary & Elbaz 2001) have the feature that they can be constrained by counts and the cosmic background radiation in various IR and submm bands simultaneously. This is achieved by using SED templates to link sources in different bands. The SED library of Xu et al. (2001) contains realistic SEDs of a complete sample of 837 IRAS $25\mu m$ selected galaxies, enabling prediction of counts as well as color distributions, which provide additional constraints to the model. Templates in Rowan-Robinson (2001), Xu et al. (2001) and Chary & Elbaz (2001) extend from the IR-submm to optical and UV wavebands, hence these models can predict also the contributions from IR sources to optical and UV counts, relating the evolution of IR sources to that of galaxies seen in earlier optical and UV surveys. All of these works found strong evolution among IR sources in the redshift range of $0 < z < 1.5$. Assuming that the narrow sub-mJy bump on the Euclidian normalized differential counts of ISOCAM $15\mu m$ surveys (Elbaz et al. 1999) is due to the K-corrections caused by the strong unidentified broad band emission features (UIB) at $6 - 8\mu m$, which are shifted into the ISOCAM $15\mu m$ band filter (LW3) when $z \sim 1$, Xu (2000) concluded that typical IR galaxies at $z \sim 1$ have $L_{15\mu m} \sim 10^{11} L_{\odot}$, namely about 20 times more luminous than their local counterparts, while their comoving density is about the same as their local counterparts. As argued by Xu et al. (2001), the location of the $15\mu m$ bump ($f_{15\mu m} \sim 0.4 mJy$) provides a strong constraint on the luminosities of IR sources at $z \sim 1$. This has been confirmed by the detailed study of ISOCAM sources in the HDF-north by Elbaz et al. (2002), who obtained redshifts for nearly all of these sources (40 out of total 41). The strong evolution has also been supported by surveys in other ISOCAM bands. For example, Clements et al. (2001) found that the luminosity functions of their ISO $12\mu m$ sources are consistent with a pure luminosity evolution of rate $\sim (1 + z)^{4.5}$, as derived by Xu (2000) from the ISOCAM $15\mu m$ counts.

On the other hand, different authors identified different populations of galaxies as the major carriers of the evolution of IR sources. It was found in early IRAS studies

(Franceschini et al. 1988; Rowan-Robinson & Crawford 1989) that IR sources can be divided into 3 different populations: normal late-type galaxies ('cirrus galaxies'), starburst galaxies, and galaxies with AGNs. Assuming that all IR sources undergo pure luminosity evolution with the same evolution rate, Rowan-Robinson (2001) found that 'cirrus galaxies' dominate the ISOCAM $15\mu m$ counts, the SCUBA $850\mu m$ counts, and the cosmic IR background radiation. Xu et al. (2001), motivated by results of optical identifications of ISO galaxies by Flores et al. (1999b) and Aussel et al. (1999) which show a larger percentage of these sources are in interacting systems, assumed that most of the evolution of the IR sources is due to starburst galaxies (defined by warm FIR colors: $f_{60\mu m}/f_{100\mu m} \geq 0.5$). Obscured AGNs with relatively low $f_{25\mu m}/f_{60\mu m}$ ratios (due to the very high extinction affecting even the MIR fluxes) may be misclassified as starbursts in Xu et al. (2001), who classified galaxies with AGNs using the criterion $f_{25\mu m}/f_{60\mu m} \geq 0.2$. Franceschini et al. (2001) also assumed that the strong evolution is confined to the starburst population. Their starburst galaxies include all 'active' galaxies not classified as Sey 1, i.e. including the Sey 2s and the LINERs, in Rush et al. (1993). Pearson (2001) found that a separate population of ultra-luminous galaxies (ULIRGs) with $L \sim 10^{12} L_{\odot}$, confined in a very narrow range of redshift centered at $z \sim 1$, is mostly responsible for the strong evolution seen in the ISOCAM $15\mu m$ counts. Since all these models can fit the IR-submm counts and the CIB within uncertainty limits, there is apparently a degeneracy concerning the population of galaxies that carry most of the evolution of IR sources. The degeneracy still remains even when the new, detailed information of the 15 micron universe (source counts, redshift distributions, luminosity functions at different redshifts, etc.; Elbaz et al. 2002; Franceschini et al. 2001) is considered (see Section 2).

One of the central issues in the current agenda of hierarchical galaxy formation simulation studies concerns the roles played by two different star formation modes (eg. Somerville et al. 2001; Kauffmann et al. 2001), namely the quiescent star formation mode

and the interaction-induced star formation mode. There are apparent links between the normal quiescent galaxies and the quiescent star formation (as in the Milky Way and M31) and between starburst galaxies and the interaction-induced star formation (as in the Antennae Galaxies and in M82). Therefore, the answer to the question whether the normal galaxies or starburst galaxies dominate the faint IR counts will have important impact on galaxy evolution theories.

Another deficiency of the current models for IR sources is the neglect of early type galaxies. Although these galaxies have little dust emission, therefore do not contribute significantly to IR counts at wavelengths longer than $\sim 10\mu m$, they are found as an important population in ISO $6.7\mu m$ counts (Flores et al. 1999b; Aussel et al. 1999; Serjeant et al. 2000). Future mid-IR surveys such as those planned for SIRTf IRAC cameras (4 bands centered at $3.6\mu m$, $4.5\mu m$, $5.8\mu m$ and $8\mu m$, respectively) will certainly detect many of these galaxies.

In this paper, we shall address the above two issues, namely (1) developing new models to investigate how to break the degeneracy concerning the major evolution population in IR counts (using SIRTf data in particular), and (2) modeling the evolution of E/S0 galaxies and predicting their contributions to the MIR counts. The plan of the paper is as follows: in Section 2 a set of new models for evolution of dusty galaxies are presented, while in Section 3 models for evolution of E/S0 galaxies are developed and compared to the observations; predictions for the UV, optical and NIR counts by a set of composite models, each consisting of a dusty galaxy evolution model and an E/S0 evolution model, are presented and compared with data in Section 4. The predictions for counts and confusion limits in SIRTf bands by the same models are presented in Section 5. In Section 6 we show how to use color distributions of ISO sources and future SIRTf sources to answer the question whether starburst galaxies or normal late-type galaxies are dominant in the

IR sources. Section 7 is devoted to discussion. A summary is given in Section 8.¹ The Λ -Cosmology ($\Omega_\Lambda = 0.7$, $\Omega_m = 0.3$, $H_0=75 \text{ km sec}^{-1} \text{ Mpc}^{-1}$) is assumed throughout the paper.

2. New Models for Evolution of Dusty Galaxies

2.1. Previous Models

In all the multi-band models for the evolution of dusty galaxies in the literature, the different populations of galaxies are separated by their characteristic spectral energy distributions (SEDs): the normal galaxies have relatively low $f_{60\mu\text{m}}/f_{100\mu\text{m}}$ and $f_{25\mu\text{m}}/f_{12\mu\text{m}}$ ratios and very prominent UIB features, the starburst galaxies have relatively high $f_{60\mu\text{m}}/f_{100\mu\text{m}}$ and $f_{25\mu\text{m}}/f_{12\mu\text{m}}$ ratios and less prominent UIB features over a steep rising MIR continuum, and galaxies with AGNs have relatively high $f_{25\mu\text{m}}/f_{60\mu\text{m}}$ ratios and very weak UIB (contributed by ISM dust not associated with the AGN). Models by Xu et al. (2001) have also considered the luminosity dependence of the SED in each population, while some other models (Rowan-Robinson 2000; Franceschini et al. 2001; Pearson 2001; Chary & Elbaz 2001) separate high luminosity starbursts (Arp220 type) from moderate luminosity starbursts (M82 type). Because of their different SEDs, these different populations of galaxies give different relative contributions to counts at different wavelengths. However, it appears that the counts are rather loose constraints to these relative contributions. At least 2 factors are responsible for this degeneracy: (1) there are many parameters in the evolution functions (both the luminosity evolution and the density evolution) when different populations are allowed to evolve differently, and (2) there are still significant uncertainties

¹More detailed results on predictions of models presented in this paper are available on request to C.K.X..

in the current ISO counts (e.g. counts of the same ELAIS $15\mu m$ sources reported by Serjeant et al. 2000 and by Gruppioni et al. 2002 differ with each other by as much as a factor of 3), due both to calibration errors and the field-to-field variation. In principle, the degeneracy can be broken by comparing model predictions on redshift distributions of deep FIR ($\lambda \gtrsim 60\mu m$) selected samples with observations: Models assuming warmer IR SEDs (starbursts dominant) usually predict larger mean redshifts than models assuming cooler IR SEDs (normal-galaxies dominant) do. However, similar to the SCUBA galaxies, the large beams of FIR detectors (such as the ISOPHOT cameras) make it rather difficult to pin-down the optical counterparts (usually quite faint) of faint FIR sources.

A more direct method to constrain the relative contributions of different populations to the IR counts is to compare the predicted and observed color distributions of IR sources. Among the multi-band models for evolution of dusty galaxies in the literature, those of Xu et al. (2001) have the most sophisticated algorithm in dealing with the SEDs, and are the only ones that can predict both the mean colors and their dispersions. Therefore, we choose to build our new models using the same algorithm as Xu et al. (2001).

2.2. New Models

In the new models, the simulation code of Xu et al. (2001) is modified in the following aspects:

- (1) The luminosity and density evolution functions for the starburst galaxies and normal late-type galaxies, respectively, have the following new form:

$$F_i(z) = (1+z)^{u_i} \times \left(\frac{(1+(1+z)/(1+z_1))}{(1+1/(1+z_1))} \right)^{v_i-u_i} \times \left(\frac{(1+1/(1+z_2))}{(1+(1+z)/(1+z_2))} \right)^{v_i+w_i} \quad (z \leq 7); \quad (1)$$

and

$$G_i(z) = (1+z)^{p_i} \times \left(\frac{(1+(1+z)/(1+z_1))}{(1+1/(1+z_1))} \right)^{q_i-p_i} \times \left(\frac{(1+1/(1+z_2))}{(1+(1+z)/(1+z_2))} \right)^{q_i+r_i} \quad (z \leq 7). \quad (2)$$

These smoothly-joined 3-piece power laws, in contrast with the sharply-joined 2-piece power laws used in Xu et al. (2001), will allow softening in the low redshift end ($z < 0.5$) of the evolution functions to improve the fit to the redshift distribution of IRAS $60\mu m$ sources.

- (2) The $25\mu m$ local luminosity functions (LLF) of 3 populations used in Xu et al. (2001) did not themselves take into account of the evolutionary effects. In the new models, new $25\mu m$ LLFs corrected for these effects are used (see Appendix A for the details of the new LLFs). It is found that these new LLFs are only marginally different from the old ones.
- (3) The UV portion ($\lambda < 3000\text{\AA}$) of the SEDs in the SED lib, which is an important part of the code, is better constrained in this work (Appendix B).

Given the large number of parameters, it is out the scope of this paper to explore the entire parameter space for models allowed by available data. Instead, we concentrate on three models which predict very different relative contributions by starburst galaxies and normal late-type galaxies to the counts in the IR surveys. For each of them, parameters have been fine-tuned so that the model can fit all available data as well as possible. These models for dusty galaxies are presented in Table 1 and Fig.1.

Model S1 is similar to the models in Xu et al. (2001) and in Franceschini et al. (2001) in the sense that the starburst galaxies are assumed to dominate the evolution of the IR sources. In Model S2, similar to Rowan-Robinson (2001), all three populations of dusty galaxies are assumed to have pure luminosity evolution with the same evolution rate. This

is actually the same evolutionary scenario adopted by Xu (2000), who assumed that the entire body of IR sources evolve as a single population. Note Rowan-Robinson (2001) assumes that there is no SED evolution, while in Model S2 we assume SEDs evolving with luminosity. In Model S3, it is assumed that the normal galaxies and starburst galaxies give about equal contributions to the ISOCAM $15\mu m$ counts, as hinted at by the optical identifications of ISO sources (Flores et al. 1999b; Aussel et al. 1999). For Model S1 and Model S3, the luminosity evolution function of galaxies with AGNs is adopted from the optical QSO luminosity evolution function of Boyle et al. (2000)

$$F_{AGN}(z) = 10^{1.36z - 0.27z^2} \quad (z \leq 7). \quad (3)$$

This is slightly different from the power law function used in Xu et al. (2001).

Table1. New models for dusty galaxies

model			Normals			Starbursts						AGNs		
	z_1	z_2	u_1	v_1	w_1	u_2	v_2	w_2	p_2	q_2	r_2	u_3	v_3	w_3
S1	0.5	0.85	1.5	1.5	2	2	11.5	1.2	1	9.8	1.2	$1.36z - 0.27z^2$		
S2	0.5	1.2	3.2	5.7	2.5	3.2	5.7	2.5	0	0	0	3.2	5.7	2.5
S3	0.5	1	2	8	2	2	10.2	1.5	2	3	1.5	$1.36z - 0.27z^2$		

2.3. Predictions for Counts and Redshift Distributions

In Fig.2, Fig.3 and Fig.4, predictions by these 3 models for the $15\mu m$, $60\mu m$, $90\mu m$, $170\mu m$, $850\mu m$ counts and for the CIB are compared with the data ², respectively. The data points are taken from a large pool of measurements found in the literature, which is still evolving rapidly. This is particularly true for the measurements involving ISO data, because more and more new data reduction tools are becoming available for these rather complex data.

Model S1, which is otherwise same as the 'peak model' in Xu et al. (2001) except for the modifications listed in Section 2.2, predicts that the contribution from the starburst population dominates almost everywhere in these plots. The model predictions are in reasonably good agreements with data in all plots, given the large dispersions in the data sets. Particularly, the new results of Gruppioni et al. (2002) on the $15\mu m$ counts of ELAIS sources (filled 4-point stars in plot) are about a factor of 3 lower than the counts from the same survey reported by Serjeant et al. (2000) (open 4-point stars), and are also significantly lower than other ISOCAM measurements in the flux range of $1 \text{ mJy} < f_{15\mu m} < 10 \text{ mJy}$. Model S1 predicts a less prominent sub-mJy peak in the $15\mu m$ counts than the 'peak model' of Xu et al. (2001), because the sharp peak at $z=1.5$ in the evolution functions of the old model is replaced by a smooth peak in the new model (at $z \simeq 1.3$, see Fig.1). It is worth to note that, in the bright end of the SCUBA counts ($f_{850\mu m} \gtrsim 5 \text{ mJy}$), the model predicts that the contribution from galaxies with AGN exceeds that from starbursts. This result seems to be consistent with the limited knowledge we have about the bright SCUBA

²The units used in the plots throughout this paper are rather heterogeneous. This is because many data points collected from the literature are measured from figures that used different units. Often it is difficult to convert them to the same units, in particular for errors bars.

sources: out of the 7 SCUBA sources of $f_{850\mu m} \geq 8mJy$ in the sample of Smail et al. (2002), 4 show signs of AGN. On the other hand, the model predictions on the SCUBA $850\mu m$ counts are close to the lower boundary of the data.

In contrast to Model S1, Model S2 predicts that for $15\mu m$ counts, $850\mu m$ counts and for the CIB, the population of normal galaxies dominate (Fig.3). This is in agreement with the results of Rowan-Robinson (2001). The same model predicts that normal galaxies and starburst galaxies give about equal contributions to the $170\mu m$ counts, and starbursts dominate the $90\mu m$ and $60\mu m$ counts. This model can also fit the data in all these plots well (Fig.3).

By design, the contributions from normal galaxies and from starburst galaxies are indeed nearly equal in the predictions of Model S3 for $15\mu m$ counts (Fig.4). The same model predicts that the $60\mu m$, $90\mu m$ and $170\mu m$ counts are dominated by starbursts. For the SCUBA $850\mu m$ band, the model predicts comparable contributions from the normal galaxies and from the starbursts to the counts in a wide flux range, and the contribution from AGNs dominant the counts at a few 10s of mJy level while being negligible at sub-mJy level. The CIB predicted by this model is dominated by the contribution from the starbursts in the wavelength range $20\mu m \lesssim \lambda \lesssim 300\mu m$, and by that from normal galaxies at other wavelengths.

In Fig.5, Fig.6 and Fig.7, predictions by the 3 models for the redshift distributions for the IRAS $60\mu m$, ISOCAM $15\mu m$, ELAIS $90\mu m$, FIRBACK $170\mu m$, and SCUBA $850\mu m$, and future SWIRE $24\mu m$ surveys are plotted. The model predictions for the IRAS $60\mu m$ and ISOCAM $15\mu m$ surveys are compared to the data. All 3 models give more satisfactory fits to redshift distribution of the IRAS $60\mu m$ sources than the ‘peak model’ (favorite model) of Xu et al. (2001) does, though Model S1 still over-predicts the number of IRAS $60\mu m$ sources with $z > 0.2$ by about a factor of 3. For the redshift distribution of ISOCAM

$15\mu m$ sources in the HDF-north, the predictions of the Model S1 gives the best fit among the 3 models although, given the large error bars of the data, the difference among model predictions is subtle.

All the 3 models predict bi-modal redshift distributions for ELAIS $90\mu m$ and FIRBACK $170\mu m$ sources, with normal galaxies dominating the first peak and starburst galaxies dominating the second peak. Model S1 predicts that most of ELAIS $90\mu m$ and FIRBACK $170\mu m$ sources have $z \geq 0.5$. In contrast, Model S2 predicts that most of these sources have $z \leq 0.5$, being in the first peak of the redshift distributions. This difference is due to the so-called 'temperature-redshift' degeneracy for infrared galaxies (Blain 1999): In the long wavelength bands such as the $90\mu m$ and the $170\mu m$, the sources in Model S1 tend to have larger redshifts than those in Model S2 in order to compensate their warmer IR SEDs. Interestingly, this indicates that we can break the degeneracy over these models by comparing the predicted and observed redshift distributions of the ISOPHOT sources in these bands. Serjeant et al. (2001) obtained high confidence redshifts for 16 (out of 37) sources of $f_{90\mu m} \geq 0.1Jy$ in the ELAIS S1 field (3.96 deg^2), none of them has redshift larger than 0.5. This sets a lower limit of $43 \pm 11\%$ for the percentage of the $90\mu m$ sources in this field to have $z < 0.5$. Taken at the face value, only the prediction of S2 (53%) is comfortably above this lower limit, while the prediction of S3 (37%) is marginally consistent with it, and the prediction of S1 (30%) is marginally below the limit. The above comparisons seem to favor Model S2. However, given the fact that this data set was taken from a small region and can be seriously affected by any clustering effect, more observations are needed for any definitive conclusions.

Model S1 predicts a broad redshift distribution, peaking between $2 < z < 3$, for bright SCUBA sources ($f_{850\mu m} > 8 \text{ mJy}$), broadly consistent with observational constraints (Smail et al. 2002; Ivison et al. 2002; Fox et al. 2002). For the same sources, Model S2 predicts a

prominent peak around $z=1.5$ and less than 25% of sources at redshifts > 2 , not favored by observations which in general suggest a mean redshift larger than 2 (see, e.g. Ivison et al. 2002). Model S3 also predicts a peak around $z=1.5$ for the $f_{850\mu m} > 8$ mJy sources, though with a much wider high-redshift wing (44% of sources have $z \geq 2$).

2.4. Predictions for ISO LFs and SFH

The ISOCAM $15\mu m$ sources in HDF-North have been thoroughly studied in the literature (Rowan-Robinson et al. 1997; Aussel et al. 1999; Elbaz et al. 1999; Cohen et al. 2000; Franceschini et al. 2001; Elbaz et al. 2002). All but 1 of a total of 41 sources with $f_{15\mu m} \geq 0.1$ mJy have spectroscopic redshifts (Franceschini et al. 2001; Elbaz et al. 2002). Exploiting these redshifts, we derived the $15\mu m$ luminosity functions (LFs) in three redshift intervals: $0.4 < z \leq 0.7$, $0.7 < z \leq 1$, and $1 < z \leq 1.3$ using the classical V_{max} method. These results are compared to the predictions of the three models in Fig.8.

Given the small size of the data set (40 galaxies), it is understandable that the derived luminosity functions have substantial uncertainties. Particularly, significant fluctuations can be found in the redshift distributions (Fig.5–7), presumably due to clustering effects. Compared to these uncertainties, the difference in the predictions by the three different models is again subtle. They all lie near the lower ends of the error-bars (Poisson error) of the two data points in the panel of $0.4 < z < 0.7$. This is likely to be due to a bias in the data caused by the over-density in the $0.4 < z < 0.6$ bin (Fig.5–7). In the panels of $0.7 < z < 1$ and $1 < z < 1.3$, the predictions of Model S1 are slightly higher and fit the data slightly better than those of other two models.

In Fig.9a, the star formation history (SFH) predicted by the three models are compared to observations. The red lower limits are derived from the ISOCAM $15\mu m$ LFs (Fig.8).

The lower limit of $15\mu m$ luminosity density is derived by summing up the contributions in the bins where the LF is actually measured (i.e. no extrapolations are applied to *measured* LFs), then converted to total IR luminosity using the formula $L_{ir} = 11.1 \times L_{15\mu m}$ (Elbaz et al. 2002). The star formation rate is then estimated from the IR luminosity density using the formula of Kennicutt (1998): $SFR (M_{\odot} \text{ yr}^{-1}) = L_{ir} \times 1.7 \cdot 10^{-10} L_{\odot}$. The predictions of the three models are very close to each other (within 50%).

In Fig.9b, Fig.9c and Fig.9d, these predictions are broken into contributions by different populations. Indeed Model S1 predicts that, except for in the low z end ($z \lesssim 0.2$), the starburst galaxies overwhelmingly dominate the star formation in the universe. Model S2 predicts just the opposite: the star formation in the universe has been always dominated by normal late-type galaxies, while in Model S3 the contributions of these two populations are more comparable. All three models predict minor contributions from galaxies with AGNs. Note that since some of the IR emission from galaxies with AGNs is powered by the gravitational energy released in the AGN, not by star formation, the model predictions plotted here should be treated as upper limits.

In the literature, the steep decline of the star formation rate since $z \sim 1$ has been well established since early works of Lilly et al. (1996) and Madau et al. (1996). However, it is still controversial on what happened to the star formation rate in earlier universe, particularly before $z = 2$. Most information on this issue is obtained from observations of Lyman-Break galaxies (LBGs, Steidel et al. 1999). However, the extinction correction for these rest-frame UV selected galaxies is very uncertain. In addition, many high redshift star-forming galaxies may be completely missed in the surveys of LBGs because of heavy extinction, causing systematic underestimation when using LBGs to determine the star formation rate in high z universe (see, e.g., Rowan-Robinson et al. 1997). In this respect, the predictions of our models follow closely the data points determined from LBG surveys

after the extinction correction (Steidel et al. 1999). As discussed in Xu et al. (2001), the evolution of IR galaxies at redshifts > 2 is mainly constrained by the sub-mm data in the SCUBA surveys and in the CIB observations, due to the negative K-correction. Too much star formation in those large redshifts will result in too many sub-mm counts and too high sub-mm background radiation. In the literature, other models (e.g. Gispert et al. 2000; Rowan-Robinson 2000; Chary & Elbaz 2001) which also invoked sub-mm data to constrain the evolution of $z > 2$ IR galaxies found the similar trend (a peak at $z \sim 1$ and a shallow/flat slope in $z \gtrsim 2$) in the SFR evolution. The claim that the universal star formation rate increases monotonically with redshift to very high z ($\gtrsim 7$) by Lanzetta et al. (2002) is not supported by our and other studies on evolution of IR galaxies.

3. Passive Evolution Models for E/S0 Galaxies

The models follow a simple, passive evolution approach (Pozzetti et al. 1996). The basic assumption is that there has been no star formation in an E/S0 galaxy since its initial formation. Consequently, its radiation in different bands (i.e. the SED and the L/M ratio) evolves passively with the ever-aging stellar population. Instead of assuming that all E/S0's formed at once together (as in the classical monolithic galaxy formation scenario), the E/S0 galaxies are assumed to form in a broad redshift range (Franceschini et al. 1998), specified by a truncated Gaussian function. The SEDs of different ages are calculated using the GRASIL code of Silva et al. (1998). No dust emission is considered in these models.

3.1. Evolution Function

The evolution function $\Psi(M, t)$, specifying how many E/S0s are formed in a unit volume, in a unit time interval, and in a unit mass interval, is assumed to have the following

form:

$$\Psi(M, t) = \psi(M) T(t) \quad (4)$$

where the time dependence function $T(t)$ is a truncated Gaussian:

$$\begin{aligned} T(t) &= \exp(-(t - t(z_{peak}))^2/\omega^2) & (t \geq t(z_0)) \\ &= 0 & (t < t(z_0)). \end{aligned} \quad (5)$$

In this prescription, for the sake of simplicity, the time dependence is assumed to be independent of the mass. This implies that E/S0s of different mass have the same formation history (i.e. no differential evolution). The time dependence function $T(t)$ is fully defined by 3 free parameters: the peak formation time $t(z_{peak})$, the time scale ω (in Gyr), and the time when the formation of E/S0s started $t(z_0)$.

Accordingly, for a given redshift z , the number of E/S0's in a unit mass interval and a unit volume can be found from the following integration:

$$\Phi(M, z) = \psi(M) \int_{t(z_0)}^{t(z)} T(t') dt'. \quad (6)$$

If the local mass function $\Phi(M, z = 0)$ is known, then the mass dependence function $\psi(M)$ can be derived:

$$\psi(M) = \frac{\Phi(M, z = 0)}{\int_{t(z_0)}^{t(z=0)} T(t') dt'}. \quad (7)$$

where $t(z = 0)$ is the current age of the universe.

In this work, the local mass function is constrained using the local K-band luminosity function of Kochanek et al. (2001) and the L_K/M ratio predicted by GRASIL code (Silva et al. 1999).

3.2. Galaxy Age Distribution and SED Assignment

Eq(6) predicts galaxy number for a given redshift in a unit mass interval and a unit volume. These galaxies have different ages spanning between $\tau = 0$ and $\tau = t(z) - t(z_0)$. The age distribution function, $G(z, \tau)$, is also a truncated Gaussian:

$$\begin{aligned} G(z, \tau) &= G_0 \exp(-(t(z) - \tau - t(z_{peak}))^2/\omega^2) & 0 \leq \tau \leq (t(z) - t(z_0)) \\ &= 0 & (otherwise). \end{aligned} \tag{8}$$

For every galaxy simulated, an age is assigned to it according to the above distribution (i.e. probability) function. According to the passive evolution model, galaxies of different ages have different SEDs and different L/M ratios. The SEDs of different ages are calculated using GRASIL (Silva et al. 1998). Again, for the sake of simplicity, we assume a simple ‘single-burst’ scenario, in analogy to the merger scenario of E/S0 formation as hinted at in the studies of ULIRGs (Kormendy & Sanders 1992), to model the formation of E/S0s. Namely, we assume that all the stars in an E/S0 galaxy were formed in a short burst (lasting 10^8 yrs), after which all the ISM was blown out. Accordingly, the following parameters are adopted for the input of GRASIL: $t_{win} = 0.1$ (Gyr), $k_{sch} = 1.0$, $\nu_{sch} = 20.0$, and $\tau_{inf} = 0.01$. Then, in the simulation of E/S0s, we include only sources older than 1 Gyrs. Here we implicitly assume that merger remnants younger than 1 Gyr do not look like E/S0s because these systems may have not fully relaxed. Namely they should be classified as post-starbursts or E+As, not E/S0s. Optical follow-up observations of ISOCAM sources (Flores et al. 1999b; Aussel et al. 1999; Cohen et al. 2000; Elbaz et al. 2002) have shown that E+A galaxies are IR bright and have similar IR properties as active starburst galaxies.

3.3. Three Models for E/S0 Evolution

We consider 3 different E/S0 models in this paper, specified by different z_{peak} and ω (Table 2, Fig.10). Model E1 ($z_{peak} = 5$, $\omega = 0.5$ Gyr) mimics the classical monolithic scenario (Eggen et al. 1962). Model E2 assumes a later and broader E/S0 formation epoch ($z_{peak} = 2$, $\omega = 2$ Gyr). Model E3 ($z_{peak} = 1$, $\omega = 3$ Gyr) assumes that most of E/S0s are formed at $z > 1$, as hierarchical galaxy formation workers have advocated (Kauffmann et al. 1993; Kauffmann & Charlot 1998).

Table 2. Evolution models for E/S0s

Models	z_{peak}	ω (Gyr)	z_0
E1	5	0.5	7
E2	2	2	7
E3	1	3	7

In Fig.11 we compare the model predictions on the redshift dependence of optical/NIR colors with the data from Franceschini et al. (1998). Predictions of all three models can fit the overall trend of the data well. On the other hand, Model E1 predicts very little scattering, which is not confirmed by the data. The other two models predict significantly larger dispersion, in better agreement with the data.

In Fig.12 the redshift distribution of early type galaxies of $K_{ab} \leq 20.15$, taken from

Franceschini et al. (1998), is compared to the model predictions. Note that only 15 out of 35 redshifts in Franceschini et al. (1998) are spectroscopically measured, the rest are photometric redshifts. Among the three models, Model E2 fits the data best. It should be noted that, as discussed in Benitez et al. (1999) and Rodighiero et al. (2001), some high z E/S0s may have been missed in the Franceschini et al. (1998) investigation.

4. Counts in UV, Optical, NIR and MIR Bands

Both the E/S0 galaxies and the dusty galaxies contribute significantly in these bands. Since the three E/S0 models predict almost identical counts (difference $\lesssim 0.1$ dex), in the rest of the paper we shall present only the results from Model E2 ($z_{peak} = 2$, $\omega = 2$ Gyr).

In Fig.13, Fig.14 and Fig.15 the contributions of E/S0 galaxies to the counts in these bands (as predicted by Model E2) are added to the contributions of dusty galaxies as predicted by Model S1, Model S2 and Model S3, respectively. These model predictions are compared to observations in the vacuum UV (2000Å), the B and R, the NIR K, and the MIR 6.7 μm band (ISOCAM) and 12 μm (IRAS and ISO CAM) bands. Between the three figures, the differences in the total counts in the bands plotted are generally within the uncertainties of data. The model predictions can account for all counts in the R, K and MIR bands. On the other hand, the model predictions are significantly lower than the counts observed in the 2000Å band (Milliard et al. 1994). For the B band, the model predictions are slightly lower (~ 0.3 dex) than the observed counts for $B > 20$ mags. These results strongly hint at a population of star forming galaxies which are infrared quiet (very low dust attenuation/emission), therefore seen only in the UV and the blue bands (see Section 7.3 for more discussion).

In the bright end of the K-band counts, the prediction by S1+E2 (Fig.13) is in good

agreement with the morphologically segregated counts reported by Huang et al. (1998), namely at $K \lesssim 17$ the E/S0 galaxies contribute about 50% of the counts, and at fainter magnitudes the contribution from late-types becomes more and more dominant. The predictions by S2+E2 and S3+E2 on the E/S0 contribution to K-band counts at $K=16$ are $\sim 30\%$ and $\sim 40\%$, slightly less than the observational result of Huang et al. (1998).

The three models fit the faint, sub-mJy ISOCAM $6.7\mu m$ counts very well. However, predictions of S1+E2 are about a factor of 3 lower than the ELAIS counts (Serjeant et al. 2000) at few mJy level. For these counts, predictions by S3+E3 have the best agreement with, though being still about 50% less than, the data. It should be noted that, as indicated by the large discrepancy between the ELAIS $15\mu m$ counts of Serjeant et al. (2000) and of Gruppioni et al. (2002), the uncertainties of the ELAIS $6.7\mu m$ counts of Serjeant et al. (2000) may be significantly larger than reported.

The scatters of the ISOCAM $12\mu m$ data (Clements et al. 1999) are large, indicating significantly larger uncertainties than the Poisson noise (error bars in the plot). The three brightest ISO points may suffer serious biases caused by errors in galaxy/star separation (Clements et al. 1999), so are likely to be less reliable than other data points. If this is indeed the case then, among the three models, the predictions of S1+E2 have the best agreement with the data. The effect of the Local Supercluster (Lonsdale et al. 1990) can be seen in the bright IRAS $12\mu m$ counts.

5. Counts and Confusion Limits in SIRTf Bands

The E/S0 galaxies contribute significantly only to the four IRAC bands ($3.6\mu m$, $4.5\mu m$, $5.8\mu m$, and $8\mu m$), while the 3 MIPS bands ($24\mu m$, $70\mu m$ and $160\mu m$) will see only dusty galaxies.

Model predictions of contributions by E/S0 galaxies and by different populations of dusty galaxies to the counts in three SIRTf bands ($3.6\mu m$, $24\mu m$ and $70\mu m$ bands) are plotted in Fig.16. The total counts by the three different models are very close to each other, though the relative contributions from normal galaxies and from starbursts are very different. This can be understood by the fact that, tuned to fit the same counts in the ISO bands which covers a wide wavelength range from $6.7\mu m$ to $170\mu m$, these models are forced to be similar with each other.

The $3\text{-}\sigma$ confusion limits are given in Table 3 for all 7 SIRTf bands. These are calculated by the method described in Xu et al. (2001), and assuming that SIRTf (85 cm dish) is diffraction limited in all bands (so the beams can be approximated by the Airy function). Since this idealized assumption may not be true, particularly for the short wavelength IRAC bands (e.g. the $3.6\mu m$ and $4.5\mu m$ bands), the results for those bands should be treated as lower limits. The confusion limits predicted by the 3 different models differ by up to 80%. The largest difference occurs for the $70\mu m$ band. These differences reflect the real uncertainties, mostly due to the uncertainties in the ISO data which are the major constraints to the models.

Table 3. Confusion limits (3σ) of SIRTf bands

Models	$3.6\mu m$	$4.5\mu m$	$5.8\mu m$	$8\mu m$	$24\mu m$	$70\mu m$	$160\mu m$
S1+E2	0.12 μJy	0.21 μJy	0.43 μJy	1.02 μJy	65 μJy	6.15 mJy	81.5 mJy
S2+E2	0.18 μJy	0.35 μJy	0.65 μJy	1.32 μJy	57 μJy	3.35 mJy	57.5 mJy
S3+E2	0.14 μJy	0.27 μJy	0.53 μJy	1.17 μJy	57 μJy	4.45 mJy	68.5 mJy

6. Colors as Model Discriminators for Dusty Galaxies

In empirical evolution models, different populations of dusty galaxies are distinguished by different SEDs. Therefore, the most direct method to distinguish models predicting different dominant populations for IR sources is to compare the predicted color distributions with the observations.

In Fig.17, we compare predictions of the three models for evolution of dusty galaxies (Table 1) for colors of ISO galaxies. The detection limits are set to be $f_{6.7\mu m} \geq 30 \mu Jy$, $f_{15\mu m} \geq 100 \mu Jy$, $f_{90\mu m} \geq 100 mJy$, $f_{170\mu m} \geq 180 mJy$, $R \leq 24 mag$, and $K \leq 20 mag$. The predictions for $f_{15\mu m}/f_R$ and $f_{15\mu m}/f_K$ are compared to the data of ISOCAM $15\mu m$ sources in HDF-N (Aussel et al. 1999; Cohen et al. 2000; Hogg et al. 2000). It appears that, for ISO galaxies, only the $f_{15\mu m}/f_K$ color is a good model discriminator in the sense that the peaks of the color distributions predicted by the three models are separated from each other. The data seem to favor Model S1 which predicts a peak in the $f_{15\mu m}/f_K$ color distribution right at the place where the data peaks. However, this data set is again too small (30 galaxies) and error bars too large to distinguish the three models.

SWIRE³, a SIRTf Legacy Science program, will survey 65 deg² of sky in all 7 SIRTf bands (3.6, 4.5, 5.8, 8, 24, 70, and 160 μm) down to a depth comparable to, or even deeper than, that of ISOCAM $15\mu m$ surveys. The documented 5σ sensitivity limits of SWIRE are: $f_{3.6\mu m} = 7.3 \mu Jy$, $f_{4.5\mu m} = 8.7 \mu Jy$, $f_{5.8\mu m} = 27.5 \mu Jy$, $f_{8\mu m} = 32.5 \mu Jy$, $f_{24\mu m} = 0.45 mJy$, and $f_{70\mu m} = 2.75 mJy$, $f_{160\mu m} = 17.5 mJy$. Compared to predicted confusion limits in Table 3, it appears that SWIRE surveys will be confusion limited in the the 70 μm and 160 μm bands. Extensive ground based follow-up observations in the optical, NIR and radio bands will be carried out. These survey areas will also be observed in the far-UV (1500Å

³<http://www.ipac.caltech.edu/SWIRE>.

and 2300\AA) by GALEX⁴ in the deep survey mode. In Fig.18, model predictions for the distributions of 6 colors of SWIRE galaxies are plotted. These colors are selected among many possible combinations to illustrate how the colors of SWIRE galaxies can discriminate the models. Model simulations of sky coverage of 5 deg^2 are carried out. For each plot, the samples of simulated sources are selected according to SWIRE’s sensitivity limits or, for the $70\mu\text{m}$ and $160\mu\text{m}$ bands, the confusion limits. Also it is required that $R \leq 24$ mag and $K \leq 20$ mag when the R and K band data are involved. In four ($f_{70\mu\text{m}}/f_{8\mu\text{m}}$, $f_{24\mu\text{m}}/f_{3.6\mu\text{m}}$, $f_{24\mu\text{m}}/f_{8\mu\text{m}}$, and $f_{24\mu\text{m}}/f_K$) of the six colors plotted, the peaks of Model S1 (starburst dominant) and Model S2 (normals dominant) are clearly separate. Among these, the peak of the distribution predicted by Model 3 (intermediate model) is close to that of S1 in the $f_{70\mu\text{m}}/f_{8\mu\text{m}}$ color plot, close to that of S2 in the $f_{24\mu\text{m}}/f_{8\mu\text{m}}$ color plot, and more ambiguous in the other two plots. Given the large sky coverage of SWIRE, which is 13 times of what is simulated here, it is very hopeful that these color distributions will indeed provide clues to the question of which population is dominant among IR sources.

7. Discussion

7.1. Evolution of SEDs of Starburst Galaxies

As pointed out in Xu et al. (2001), the most important assumption in our models for the evolution of dusty galaxies is that high redshift (i.e. $z \gtrsim 1$) star-forming galaxies have the same SEDs as their local counterparts when the luminosity is the same. Since our SEDs cover from the UV all the way through to the radio waveband, the validity of this assumption demands similarity between high redshift and local galaxies in many physical conditions, a requirement that seems too strong to be fulfilled in the strict sense.

⁴<http://www.srl.caltech.edu/galex>.

Particularly, the long term star formation history plays an important role in the optical and NIR emission of galaxies, and it is obvious that high redshift galaxies have very different long term star formation history (i.e. much younger) than that of local galaxies. Does this mean that our predictions for the optical/NIR flux densities of high redshift dusty galaxies are flawed and therefore unreliable? Our argument to dispute this suspicion is based on the fact that high redshift galaxies (particularly IR selected galaxies), already detected or to be detected in the future surveys, are almost exclusively high luminosity galaxies (less luminous galaxies with high redshift are too faint to be detected). As their local counterparts, these high redshift ULIRGs must host very powerful starbursts or AGNs as energy sources which contribute much of the emission even in the NIR bands ($\sim 40\%$ for the local ULIRGs, Surace et al. 2000; Scoville et al. 2000). Therefore, as far as the detectable IR sources are concerned, the difference in the underlying old population between the high redshift dusty starforming galaxies and their local counterparts does not affect very seriously our model predictions.

Recent multi-wavebands observations of SCUBA galaxies (Smail et al. 2002), Lyman-Break Galaxies (Adelberger & Steidel 2000), and ISOCAM galaxies (Flores et al. 1999a; Aussel et al. 1999; Cohen et al. 2000; Elbaz et al. 2002) are consistent with our assumption that high redshift star-forming galaxies have similar SEDs as their local counterparts, particularly when binned according to the luminosity (as stressed by Adelberger & Steidel 2000). On the other hand, some new observations hint at possible systematic differences between high redshift and local ULIRGs. The HST image of SCUBA galaxy SMM J14011+0252 (Ivison et al. 2001) shows that the star formation activity in that source is widely spread (up to a few kpc), a situation remarkably different from typical ULIRGs found in the local universe (Sanders & Mirabel 1998). Compared to centrally concentrated starbursts found in most of the local ULIRGs, galaxies with such widely distributed starbursts are expected to have less steep MIR slopes (i.e. smaller $f_{25\mu m}/f_{12\mu m}$

ratio) and cooler FIR color (i.e. larger $f_{100\mu m}/f_{60\mu m}$ ratios). This is due to the less intense radiation field (less warm dust emission in the $25\mu m$ and $60\mu m$ bands) and less dust opacity (less extinction for MIR fluxes). Indeed, Chapman et al. (2002) found that two sources detected both by the FIRBACK $170\mu m$ band survey (Puget et al. 1999; Dole et al. 2001) and by SCUBA (Scott et al. 2000), one at $z=0.91$ and the other at $z=0.46$, have significantly cooler dust temperatures ($T_{dust} \sim 30K$) compared to $T_{dust} \sim 50K$ found for typical ULIRGs such as Arp220. They argue that this may indicate the starbursts in these systems are also extended. Given the small amount of information and the possible bias for cooler galaxies due to the sub-mm selection (Chapman et al. 2002), it is still too early to tell whether high-redshift ULIRGs are systematically more extended, and therefore have SEDs closer to less luminous local interacting galaxies (such as the Antennae galaxies) which are in earlier stages along the merger sequence. Future surveys like SWIRE will address these questions.

7.2. E/S0 evolution and starburst evolution

Comparisons between predictions E/S0 evolution models and observational data (Fig.11–12) indicate that the intermediate model (Model E2), which assumes a peak formation redshift of $z_{peak} = 2$, is the favorite among the three models. This is in agreement with some previous works (Franceschini et al. 1998; Rodighiero et al. 2001; Im et al. 2002). This model can reproduce well the trend in the color- z plots and also fit the redshift distribution very well. However, particular in the B-K v.s. z plot, the data show significantly larger dispersion than the model predictions. There are two possible causes for this:

- (1) In our simple models, we have assumed that all of the E/S0s are formed through the same starburst procedure, which means their stellar populations have the same

metallicity. It is known (e.g. Worthy 1994) that local E/S0s have different metallicity which is a major cause of the different M/L ratios and colors among these galaxies. Therefore, by neglecting these effects, our models leave some of the scatters in the color distributions unaccounted for.

- (2) Some of the blue E/S0s in the data (Franceschini et al. 1998) may not be true E/S0s. According to Im et al. (2002), many of these 'blue interlopers' have strong, narrow emission lines, suggesting that they are low-mass starbursts rather than massive star-forming E/S0s.

In fact, there is still a lack of consensus in the definition of E/S0s in deep surveys. Using a strict algorithm selecting the most symmetric and smooth galaxies, Im et al. (2002) found far less blue sources among their E/S0 sample than, e.g., Schade et al. (1999) and Menanteau (1999) whose samples were selected with less strict algorithms. A related uncertainty in our models is the choice on the exclusion of galaxies younger than 1 Gyr (Section 3.2). This choice is not entirely arbitrary: pushing the cut-off toward younger ages means more galaxies with high L/M ratios, which in turn results in too high model predictions for optical and NIR counts. This shows that the question of where to put the boundary between E/S0s and post-starbursts deserves more investigation.

If indeed E/S0s are formed through mergers (Toomre 1978; Kormendy & Sanders 1992), then their evolution is linked to the evolution of starburst galaxies which are closely related to mergers (Sanders & Mirabel 1998). Our results indeed indicate some synchronization between the two populations, in the sense that the peak of the formation function of E/S0s in the best fit model ($z_{peak} = 2$) is close to the peak of the evolution functions of starburst galaxies ($z_{peak} = 1.4$). Future works exploring this possible link will provide important constraints to the evolution of both populations.

7.3. IR-quiet star-forming galaxies

Our results (Fig. 13 – 15) show that only a small fraction (10 – 20 %) of UV selected galaxies (as in the sample of FOCA survey, Milliard et al. 1992) are IR bright, as indicated by the small contribution of simulated dusty galaxies to the UV counts (the E/S0 galaxies contribute even less). This suggests a separate population of IR quiet, UV bright galaxies which dominate the UV selected samples. Such a population is also needed for the B-band counts, because our simulations under-predict 30 – 50% of observed counts in that band, while fully account for the R and K band counts (Fig. 13 – 15). The best candidates for such galaxies are the low-metallicity (therefore low dust content) blue dwarf galaxies such as I Zw 18 (Searle & Sargent 1972). There is an apparent link between this IR quiet star-forming galaxy population and the 'faint blue galaxies' found in deep optical surveys (see Koo & Kron 1992 and Ellis 1997 for reviews). What is the relation between this population and the dusty (IR bright) star-forming galaxies? How does this population evolve (backwardly) with the redshift, and how does this evolution correlate with the evolution of IR bright galaxies? Are Lyman Break Galaxies, being selected by the UV flux in the rest frame, more closely related to the IR quiet star forming galaxies, or to the dusty star forming galaxies (as argued by Adelberger & Steidel 2000)? Answers to these questions will help to unify the pictures of galaxy formation/evolution seen in different wavebands. We plan to address these questions in our future work, particularly in connections with the forthcoming GALEX and SWIRE missions.

8. Summary

New models for the evolution of extragalactic IR sources are presented in this paper. The models for dusty galaxies and for E/S0 galaxies, the latter contributing significantly to counts at wavelengths $\lambda < 10\mu m$, have been developed separately.

Compared to previously published models in Xu et al. (2001), the new models for evolution of dusty galaxies in this work have the following improvements:

- (1) The evolution functions have the form of smoothly-joined 3-piece power-law (Fig.1), instead of the sharply-joined 2-piece power-law.
- (2) New local luminosity functions at $25\mu m$, which take into account the evolution effects, are used for the three dust galaxy populations (i.e. normal late-type galaxies, starburst galaxies, and galaxies with AGNs).
- (3) The UV portion ($\lambda < 3000\text{\AA}$) of the SEDs in the SED library is constrained by an empirical correlation between $f_{UV} - f_B$ and $B - K$, instead of mere an extrapolation of the optical SED ($\lambda > 4000\text{\AA}$).

In order to address the question whether normal late-type galaxies or starburst galaxies dominate among IR sources of $z > 0.5$, three new models are developed:

- Model S1 — starburst galaxies dominant ;
- Model S2 — normal galaxies dominant;
- Model S3 — intermediate between S1 and S2.

Predictions of these three models for counts in various bands are fairly close to each other, therefore they can hardly be distinguished using the counts. They can also fit very well the luminosity functions of ISO $15\mu m$ sources in three redshift intervals ($0.4 < z \leq 0.7$, $0.7 < z \leq 1$, $1 < z \leq 1.3$). In principle, they can be distinguished by redshift distributions of FIR sources, but the large beams of FIR detectors (such as the ISOPHOT cameras) make it rather difficult to pin-down the optical counterparts (usually very faint) of faint FIR sources. At the same time, the peaks in the distributions of several IR and optical

colors predicted by these models have separated locations. We argue that these color distributions are the best tools to distinguish these models. There are only very limited amount of multi-waveband data available for high redshift dusty galaxies in the literature (mostly for ISOCAM $15\mu m$ sources), a situation that will be drastically improved when SIRTf is launched and SWIRE surveys are available.

The models for E/S0s follow a simple, passive evolution approach. The basic assumption is that there has been no star formation in an E/S0 galaxy since its initial formation. Instead of assuming that all E/S0's formed at once together (as in the classical monolithic galaxy formation scenario), the E/S0 galaxies are assumed to form in a broad redshift range (Franceschini et al. 1998), specified by a truncated Gaussian function. The SEDs of different ages are calculated using the GRASIL code of Silva et al. (1998). No dust emission is considered in these models. Three such models with different E/S0 formation histories are calculated: Model E1 ($z_{peak} = 5$, $\omega = 0.5$ Gyr) is close to the classical monolithic scenario. Model E2 assumes a later and broader E/S0 formation epoch ($z_{peak} = 2$, $\omega = 2$ Gyr). Model E3 ($z_{peak} = 1$, $\omega = 3$ Gyr) assumes that most of E/S0s are formed at $z > 1$, as the hierarchical galaxy formation works have advocated (Kauffmann et al. 1993; Kauffmann & Charlot 1998). Comparisons with limited data (e.g. colors and redshift distribution) available for morphologically identified E/S0 galaxies at $z \sim 1$ indicate that model E2 can fit the data best among the three models. This suggests a synchronization between the evolution of E/S0 galaxies and of starburst galaxies, in the sense that the peak of the formation function of E/S0s ($z_{peak} = 2$) is close to the peak of the evolution functions of starburst galaxies ($z_{peak} = 1.4$). Combining model predictions by E2 with those by S1, S2 and S3 (dusty galaxy evolution models), comparisons with number counts in different wavebands (Fig.13–15) indicate that E/S0s contribute upto 30 – 50% of the optical/NIR counts in the bright end, and about 20 – 30% of the ISOCAM $6.7\mu m$ band counts. Their contributions to counts in the UV (2000\AA) and in the longer wavelength IR

($\geq 12\mu m$) bands are negligible.

Using these new models for extragalactic IR sources, particularly including E/S0 galaxies, we made new predictions for the counts and confusion limits in the SIRTf bands. The results indicate that SWIRE surveys will be confusion limited in the $70\mu m$ and $160\mu m$ bands. The confusion limits predicted by different models differ by up to 80%. These differences reflect the uncertainties of these predictions.

Appendix

A. New $25\mu m$ Local Luminosity Functions for Three Populations

In Xu et al. (2001), luminosity functions were presented for three population subsamples—AGNs, normal late-type galaxies and starbursts. The subsamples were determined by IRAS colors. We have extended this work to take into account the effects of luminosity evolution on the LLF estimates, and to include a more comprehensive uncertainty analysis.

We recomputed the population LLFs including a luminosity evolution term of the form $(1+z)^q$, for values of $q = 0, 3.0, \text{ and } 4.5$. This factor is applied to both the source luminosity, and the minimum luminosity detectable at the source’s redshift. The shape parameters are tabulated in Table A.1.

Table A.1. Parameters of $25\mu\text{m}$ Luminosity Functions

Population	q	α	β	L_*/L_\odot	$\alpha + \beta$
AGNs	0.0	0.336	1.691	6.9×10^9	2.027
AGNs	3.0	0.329	1.713	6.6×10^9	2.042
AGNs	4.5	0.326	1.724	6.5×10^9	2.040
Starbursts	0.0	0.265	2.283	7.9×10^9	2.548
Starbursts	3.0	0.265	2.275	7.7×10^9	2.540
Starbursts	4.5	0.264	2.300	7.9×10^9	2.564
Normals	0.0	0.482	3.875	5.7×10^9	4.357
Normals	3.0	0.480	3.992	5.8×10^9	4.472
Normals	4.5	0.479	4.055	5.8×10^9	4.534

The resulting LLFs (with same normalization constant applied) are plotted as visibilities in panel *a* of Fig.19 (solid line is no evolution; dashed is $q=3.0$; dashed-dot is $q=4.5$). There is a small difference between the LLFs at large luminosities. The model calculations in this paper use the LLFs with $q=3.0$.

We performed an analysis of the covariance of the fitted parameters, using the information matrix (Efstathiou et al. 1988). In panels *b*, *c*, and *d* of Fig.19, we have plotted the 68% confidence intervals in pairs of the parameters, as ellipses under the assumption of normally distributed uncertainties (Avni 1976; Press et al. 1992). In general, the parameters are not strongly correlated, except for α and β for AGNs. This correlation is explained by the distribution of this population at higher relative redshifts; the high-luminosity slope of

the luminosity function depends on the sum of α and β , so the parameters are degenerate when α is not well determined at low luminosities. For the same reason, the confidence intervals for AGNs for α and L_* are larger for the other populations. The variations in the parameters with evolution exponent are for the most part small compared to the uncertainties in the parameters.

B. Extrapolation of SEDs to the UV Bands

In Xu et al. (2001), the UV (1000 — 4000Å) SEDs are extrapolations from data points in the B, J, H and K bands, and therefore are not well constrained. In this work, this is improved by introducing the following constraints:

- (1) The UV-B v.s. B-K correlation. The correlation is established using a sample of galaxies detected both in the vacuum UV bands (1500Å – 2500Å) and in the FIR bands (IRAS). The sample is taken from Xu & Buat (1995). The K-band magnitudes are found in the 2MASS database. In Fig.20, the UV-B v.s. B-K color-color plot for this sample is presented. The sample is divided into galaxies with AGNs ($f_{60\mu m}/f_{25\mu m} < 0.4$), galaxies with IR excess ($f_{60\mu m}/f_{25\mu m} \geq 0.4$ and $L_{fir}/L_B > 0.5$), and normal late-types ($f_{60\mu m}/f_{25\mu m} \geq 0.4$ and $L_{fir}/L_B \leq 0.5$). Data of the three ULIRGs observed by Trentham et al. (1999) in UV using HST are also plotted. They follow the same trend of IR excess galaxies, though with larger scatters. We found that the trend for normal late-types can be well fitted by the following function

$$\begin{aligned} \log(\nu f_\nu(2000\text{\AA})/\nu f_\nu(4400\text{\AA})) &= -0.2 - 0.3 \times ((B - K) - 2)^2 && ((B - K) > 2) \\ &= -0.2 - 0.1 \times ((B - K) - 2) && ((B - K) \leq 2), \end{aligned} \quad (\text{B1})$$

and for galaxies with AGNs and galaxies with IR excess, it can be well fitted by a two-step linear function

$$\begin{aligned} \log(\nu f_\nu(2000\text{\AA})/\nu f_\nu(4400\text{\AA})) &= -0.4 \times ((B - K) - 2.) \quad ((B - K) > 2) \\ &= 0 \quad ((B - K) \leq 2). \end{aligned} \quad (\text{B2})$$

- (2) The UV slope. We use the following relation between the UV slope β ($F_\lambda \propto \lambda^\beta$, $1200\text{\AA} < \lambda < 2600\text{\AA}$) and the L_{fir}/L_B ratio, found by Calzetti et al. (1995), to constrain the slope of the UV SEDs between 1200\AA and 2600\AA :

$$\beta = 1.12 \times \log(L_{fir}/L_B) - 0.94. \quad (\text{B3})$$

- (3) Lyman-break. A sharp drop-off is imposed to the SEDs shortward of 912\AA : The flux density decreases a factor of 30 from 912\AA to 700\AA . There is a less steep drop-off, about a factor of 5, from 1200\AA to 912\AA , which is to mimic the effect of the Ly α absorption.

As an example, the model SED of M82 is compared to data in Fig.21.

This research has made use of the NASA/IPAC Extragalactic Database (NED) which is operated by the Jet Propulsion Laboratory, California Institute of Technology, under contract with the National Aeronautics and Space Administration. This work has made use of data products from the Two Micron All Sky Survey (2MASS), which is a joint project of the University of Massachusetts and the Infrared Processing and Analysis Center/California Institute of Technology, funded by the National Aeronautics and Space Administration and the National Science Foundation. C. K. Xu, C. J. Lonsdale and D. L. Shupe were supported by the SIRTf Legacy Science Program provided by NASA through a contract with the Jet Propulsion Laboratory, California Institute of Technology.

REFERENCES

- Adelberger, K.L., Steidel, C.C. 2000, *ApJ*, 544, 218.
- Altieri, B., Metcalfe, L., Kneib, J.P., McBreen, B., et al. 1999, *A&A*, 343, L65.
- Aussel, H., Cesarsky, C.J., Elbaz, D., Starck, J.L. 1999, *A&A*, 342, 313.
- Avni, Y. 1976, *ApJ*, 210, 642.
- Barger, A.J., Cowie, L.L., Sanders, D.B., et al. 1998, *Nature*, 394, 248.
- Barger, A.J., Cowie, L.L., Sanders, D.B. 1999, *ApJ*, 518, L5.
- Bertin, E., Dennefeld, M., Moshir, M. 1997, *A&A*, 323, 685.
- Blain, A.W. 1999, *MNRAS*, 309, 955.
- Blain, A.W., Smail, I., Ivison, R.J., Kneib, J.-P. 1999, *MNRAS*, 302, 632.
- Benitez, N., Broadhurst, T., Bouwens, R. Silk, J., Rosati, P. 1999, *ApJL*, 515, L65.
- Bershady, M.A., Lowenthal, J.D., Koo, D.C. 1998, *ApJ*, 505, 50.
- Boyle, B.J., Shanks, T. Croom, S.M., Smith, R.J., Miller, L., Loaring, M., Heymans, C.
2000, *MNRAS*, 317, 1014.
- Calzetti, D., Bohlin, R.C., Kinney, A.L., Stochi-Bergmann, T., Heckman, T.M. 1995, *ApJ*,
443, 136.
- Clements, D. L., Desert, F.-X., Franceschini, A., Reach, W. T., Baker, A. C., Davies, J. K.,
Cesarsky, C. 1999, *A&A*, 346, 383.
- Clements, D. L., Desert, F.-X., Franceschini, A. 2001, *MNRAS*, 325, 665.
- Chapman, S.C., Smail, I., Ivison, R.J., Helou, G., et al. 2002, *ApJ*, 573, 66.
- Chary, R.R., Elbaz, D. 2001, *ApJ*, 556, 562.
- Cohen, J.G. 2002, *ApJ*, 567, 672.

- Cohen, J.G., Hogg, D.W., Blandford, R., Cowie, L.L., Hu, E., Songaila, A., Shopbell, P., Richberg, K. 2000, *ApJ*, 538, 29.
- Dole, H., Gispert, R., Lagache, G., Puget, J-L., et al. 2001, *A&A*, 372, 364.
- Dwek, E., Arendt, R.G. 1998, *ApJ*, 508, L9.
- Dwek, E., Slavin, J. 1994, *ApJ*, 436, 696.
- Eales, S.A., Lilly, S.J., Webb, T., Dunne, L., Gear, W., Clements, D., Yun, M. 2000, *AJ*, 120, 2244.
- Efstathiou, G., Ellis, R.S., Peterson, B.A. 1988, *MNRAS*, 232, 431.
- Efstathiou, A., Oliver, S., Rowan-Robinson, M., Surace, C., et al. 2000, *MNRAS*, 319, 1169.
- Eggen, O.J., Lynden-Bell, D., Sandage, A.R. 1962, *ApJ*, 136, 748.
- Elbaz, D., Cesarsky, C.J., Fadda, D. , et al. 1999, *A&A*, 351, L37.
- Elbaz, D., Cesarsky, C.J., Chanical, P., Franceschini, A., Fadda, D., Chary, R.R. 2002, *A&A*, in press (astro-ph/0201328).
- Ellis, R.S. 1997, *ARAA*, 35, 389.
- Fang, F., Shupe, D., Xu, C., Hacking, P. 1998, *ApJ*, 500, 693.
- Finkbeiner, D.P., Davis, M., Schlegel, D.J. 2000, *ApJ*, 544, 81.
- Fixsen, D.J., Dwek, E., Mather, J.C., Bennett, C.L., Shafer, R.A. 1998, *ApJ*, 508, 123.
- Flores, H., Hammer, F., Desért, F.X., Césarsky, C., et al. 1999a, *A&A*, 343, 389.
- Flores, H., Hammer, F., Thuan, T.X., Cesarsky, C., Desert, F.X., et al. 1999b, *ApJ*, 517, 148.
- Fox, M.J., Efstathiou, A., Rowan-Robinson, M., Dunlop, J.S., et al. 2002, *MNRAS*, 331, 839.

- Franceschini, A., Aussel, H., Bressan, A., Cesarsky, C.J., Danese, L., de Zotti, G., Elbaz, D., Granato, G. L., Mazzei, P., Silva, L. 1997, in *The Far Infrared and Submillimetre Universe*; ed. A. Wilson; p.159 (Noordwijk, The Netherlands: ESA, 1997).
- Franceschini, A., Aussel, H., Cesarsky, C.J., Elbaz, D., Fadda, D., 2001, *A&A*, 378, 1.
- Franceschini, A., Danese, L., De Zotti, G., Xu, C. 1988, *MNRAS*, 233, 175.
- Franceschini, Silva, L., Fasano, G., Granato, G.L., Bressan, A., Arnouts, S., Danese, L. 1998, *ApJ*, 506, 600.
- Gardner, J. P., Sharples, R. M., Carrasco, B. E., Frenk, C. S. 1996, *MNRAS*, 282, L1.
- Gallego, J., Zamorano, J., Aragon-Salamanca, A., Rego, M. 1995, *ApJ*, 455, L1.
- Gardner, J. P., Sharples, R. M., Carrasco, B. E., Frenk, C. S. 1997, *ApJ*, 480, L99.
- Genzel, R., Cesarsky, C.J. 2000, *ARA&A*, 38, 761.
- Gilli, R., Salvati, M. and Hasinger, G. 2001, *A&A*, in press
- Gispert, R., Lagache, G., Puget, J.L. 2000, *A&A*, 360, 1.
- Glazebrook, K., Blake, C., Economou, F., Lilly, S., Colless, M. 1999, *MNRAS*, 306, 843.
- Gorjian, V., Wright, E.L., Chary, R.R. *ApJ*, 536, 550.
- Granato, G., Lacey, C.G., Silva, L. Bressan, A., Baugh, C.M., Cole, S., Frenk, C.S. 2000, *ApJ*, 542, 710.
- Gregorich, D.T., Neugebauer, G., Soifer, B.T., Gunn, J.E., Herter, T.L. 1995, *AJ*, 110,259.
- Grupponi, C., Lari, C., Pozzi, C.F., Zamorani, G., Franceschini, A., Oliver, S., Rowan-Robinson, M., Serjeant, S. 2002, *MNRAS*, 335, 831.
- Hacking, P. B., Condon, J. J., and Houck, J. R. 1987, *ApJ*, 316, L15.
- Hogg, D.W., Pahre, M.A., Adelberger, K.L., Blandford, R., Cohen, J.G., Gautier, T.N., Jarrett, T., Neugebauer, G., Steidel, C.C. 2000, *APJS*, 127, 1.

- Huang, J.-S., Cowie, L., Luppino, G. 1998, *ApJ*, 396, 31.
- Hughes, D.H., Gear, W.K., Robson, E.I. 1990, *MNRAS* 244, 759.
- Hughes, D.H., Serjeant, S., Dunlop, J., et al. 1998, *Nature*, 394, 241.
- Im, M., Simard, L., Faber, S.M., Koo, D.C., Gebhardt, et al. 2002, *ApJ*, 571, 1361.
- Iverson, R., Greve, T.R., Smail, I., Dunlop, J.S., et al. 2001, preprint (astro-ph/0206432).
- Iverson, R., Smail, I., Frayer, D.T., Kneib, J.-P., Blain, A.W. 2001, *ApJ*, 561, L45.
- Juvela, M., Mattila, K., Lemke, D. 2000, *A&A*, 360, 813.
- Kauffmann, G., White, S., Guiderdoni, B. 1993, *MNRAS*, 308, 833.
- Kauffmann, G., Charlot, S. 1998, *MNRAS*, 297, L23.
- Kauffmann, G., Charlot, S., Balogh, M. 2001, preprint (astro-ph/0103130).
- Lanzetta, K., Yahata, M., Pascarella, S., Chen, X.W., Fernandez-Soto, A. 2002, *ApJ*, 570, 492.
- Lilly, S.J., Le Fèvre, O., Hammer, F., Crampton, D. 1996, *ApJ*, 460, L1.
- Kawara, K., Sato, Y., Matsuhara, H., et al. 1998, *A&A*, 336, L9.
- Kessler, M.F., Steinz, J.A., Anderegg, M.E. et al. 1996, *A&A*, **315**, L27.
- Kochanek, C.S., Pahre, M.A., Falco, E.E., Huchra, J.P., Mader, J., Jarrett, T.H., Chester, T., Cutri, R., Schneider, S. E. 2001, *ApJ*, 560, 566.
- Koo, D., Kron, R. 1992, *ARAA*, 30, 613.
- Kormendy, J., Sanders, D.B. 1992, *ApJ*390, 53.
- La Franca, F., Matute, I., Gruppioni, C., Alexander, D. et al. 2000, to appear in the proceedings of the Fourth Italian Conference on AGNs (MemSAIt) (astro-ph/0006177).
- Lagache, G., Abergel, A., Boulanger, F., Puget, J.-L. Puget 1998, *A&A*, 333, 709.

- Lin, H., Yee, H.K., Carlberg, R.G., Morris, S.L., Sawicki, M., Patton, D.R., Wirth, G., Shepherd, C. 1999, *ApJ*, 518, 533.
- Linden-Voernle, M.J.D., Noergaard-Nielsen, H.U., Joergensen, H.E., et al. 2000, *A&A*, 395, 51.
- Lonsdale, C.J. 1999, in *Astrophysics with Infrared Surveys: A Prelude to SIRTf*, ASPC Series **177**, eds. M.D. Bica, C.A. Beichman, R.M. Cutri, and B.F. Madore, p24.
- Lonsdale, C.J., Hacking, P.B., Conrow, T.B., Rowan-Robinson, M. 1990, *ApJ*, 358, 20.
- Lonsdale, C.J., et al. 2000, http://sirtf.caltech.edu/SciUser/A_GenInfo/SSC_A1_Legacy_CL.html.
- Madau, P., Ferguson, H.C., Dickinson, M., Giavalisco, M., et al. 1996, *MNRAS*, 283, 1388.
- Malkan, M.A., Stecker, F.W. 2001, *ApJ*, 555, 641
- Matsuhara, H., Kawara, K., Sato, Y., et al. 2000, *A&A*, 361, 407.
- Mazzei, P., Aussel, H., Xu, C., Salvo, M., De Zotti, G., Franceschini, A. 2001, *New A.*, 6, 265.
- Menanteau, F., Ellis, R.S., Abraham, R.G., Barger, A.J., Cowie, L.L. 1999, *MNRAS*, 309, 208.
- Metcalfe, N., Shanks, T., Fong, R., Jones, L.R. 1991, *MNRAS*, 249, 498.
- Metcalfe, N., Shanks, T., Fong, R., Roche, N. 1995, *MNRAS*, 273, 257.
- Milliard, B., Donas, J., Laget, M., Armand, V., Vuillemin, A. 1992, *A&A*, 257, 24.
- Minezaki, T., Kobayashi, Y., Yoshii, Y., Peterson, B.A. 1998, *ApJ*, 494, 111.
- Pearson, C. 2001, *MNRAS*, 325, 1511.
- Pei, Y., Fall, S.M. 1995, *ApJ*, 454, 69.
- Pozzetti, L., Bruzual, G., Zamorani, G. 1996, *MNRAS*, 281, 953.

- Press, W.H., Flannery, B.P., Teukolsky, S.A., Vetterling, W.T. 1992, "Numerical Recipes in C: 2nd Edition", Cambridge University Press, pp. 689-699.
- Puget, J-L., Lagache, G., Clements, D.L, et al. 1999, A&A, 345, 29.
- Roche, N., Eales, S.A. 1999, MNRAS, 307, 111.
- Rodighiero, G., Franceschini, A., Fasano, G. 2001, MNRAS, 324, 491.
- Rowan-Robinson, M. 2001, ApJ, 549, 745.
- Rowan-Robinson, M., Crawford, J. 1989, MNRAS, 238, 523.
- Rowan-Robinson, M., Hughes, J., Veda, K., Walker, D.W. 1990, MNRAS, 246, 473.
- Rowan-Robinson, M., Mann, R.G., Oliver, S.J., et al. 1997, MNRAS, 289, 490.
- Rush, B., Malkan, M.A., Spinoglio, L. 1993, ApJS. 89, 1.
- Sanders, D.B., Mirabel, I.F. 1996, ARA&A, 34, 749.
- Searle, L., Sargent, W.L. 1972, ApJ, 173, 25.
- Saunders, W., Rowan-Robinson, M., Lawrence, A., et al. 1991, MNRAS, 242, 318.
- Scott, D., Lagache, G., Borys, C., Chapman, S.C., Halpern, M., Sajina, A., Ciliegi, P., Clements, D.L., Dole, H., Oliver, S., Puget, J.-L., Reach, W. T., Rowan-Robinson, M. 2000, A&A, 357, L5.
- Scott, S.E., Fox, M.J., Dunlop, J.S., Serjeant, S., et al. 2002, MNRAS, 331, 817.
- Scoville, N.Z., Evans, A.S., Thompson, R., Rieke, M., et al. 2000, AJ, 119, 991.
- Serjeant, S., Efstathiou, A., Oliver, S., Surace, C., Hraudeau, P., Linden-Vrnle, M. J. D., Gruppioni, C., La Franca, F., Rigopoulou, D., Morel, T., Crockett, H., Sumner, T., Rowan-Robinson, M., Graham, M. 2001, MNRAS, 322, 262.
- Serjeant, S., Oliver, S., Rowan-Robinson, M., Crockett, H., et al. 2000, MNRAS, 316, 768.

- Schade, D., Lilly, S.J., Crampton, D., Ellis, R.S., Le Fèvre, O., Hammer, F., Brinchmann, J., Abraham, R., Colless, M., Glazebrook, K., Tresse, L., Broadhurst, T. 1998, ApJ, 525, 31.
- Shupe, D.L., Fan, F., Hacking, P.B., Huchra, J.P. 1998, ApJ, 501, 597.
- Silva, L., Granato, G.L., Bressan, A., Danese, L. 1998, ApJ, 509, 103.
- Smail, I., Ivison, R.J., Blain, A., Kneib, J.-P. 2002, MNRAS, 331, 495.
- Soifer, B.T., Matthews, K., Djorgovski, S., Larkin, J., et al. 1994, ApJL, 420, L1.
- Somerville, R.S., Primack, J.R., Faber, S.M. 2001, MNRAS, 320, 504.
- Stanev, T., Franceschini, A. 1998, ApJ, 494, L159.
- Steidel, C.C., Adelberger, K., Giavalisco, M., Dickinson, M., Pettini, M., 1999, ApJ, 519, 1
- Surace, J.A., Sanders, D.B., Evans, A.S. 2000, ApJ, 529, 170.
- Taniguchi, Y., Cowie, L., Sato, Y., et al. 1997, A&A, 328, L9.
- Toomre, A. 1978, in IAU Symp. 79, p109.
- Trentham, N., Kormendy, J., Sanders, D.B. 1999, AJ, 117, 2152.
- Tresse, L., Maddox, S. J. 1998, ApJ, 495, 691.
- Yan, L., McCarthy, P. J., Freudling, W., Teplitz, Harry I., Malumuth, E. M., Weymann, J., Malkan, M. A. 1999, ApJ, 519, L47.
- Williams, R.E., Blacker, B., Dickinson, M., Van Dyke, W., et al. 1996, AJ, 112, 1335.
- Worthy, G. 1994, ApJS, 95, 107.
- Xu, C., Buat, V. 1995, A&A, 293, L95.
- Xu, C., Hacking, P.B., Fan, F., Shupe, D.L., Lonsdale, C.J., Lu, N.Y., Helou, G.X. 1998, ApJ, 508, 576.
- Xu, C. 2000, ApJ, 541, 134.

Xu, C., Lonsdale, C.J., Shupe, D.L., O’linger, J., Masci, F. 2001, ApJ, 562, 179.

Figure Captions:

Fig. 1.— Schematic plots of evolution functions of the three new models.

Fig. 2.— Comparisons of predictions of Model S1 with observed IR counts and CIB. Data points in the plot of $15\mu m$ counts: the ELAIS counts reported by Serjeant et al. (2000) are plotted with open four-point stars, and the ELAIS counts reported by Gruppioni et al. (2002) are plotted with filled four-point stars. Other data points have the same symbols as in Elbaz et al. (1999): A2390 (six-point stars); ISOHDF-North (open circles), ISOHDF-South (filled circles), Marano FIRBACK Ultra-Deep (open squares), Marano Ultra-Deep (exes), Marano FIRBACK Deep (asterisks), Lockman Deep (open triangles), Lockman Shallow (filled triangles). Filled squares with error bars are counts taken from Xu (2000). Note that the high points in the bright end ($f_{15\mu m} \geq 0.5$ Jy) are due to Local Supercluster (Lonsdale et al. 1990). The shaded area marks the range of counts estimated by Mazzei et al (2001). Data points in the IRAS $60\mu m$ plot: Large filled circles: Mazzei et al. (2001); Xs: Hacking & Houck (1987); open stars: Gregorich et al. (1995); open circles: Bertin et al. (1997); small filled squares: counts in the South Galactic cap ($b^{II} < -50^\circ$) by Lonsdale et al. (1990); open triangles: Saunders et al. (1991); open squares: Rowan-Robinson et al. (1990). Data points in the $90\mu m$ plot: filled circles: Efstathiou et al. (2000), crosses: Linden-Voernle et al. (2000), open square: Matsuhara et al. (2000), open diamonds: total counts of Juvela et al. (2000), open triangles: counts of multiple detections of Juvela et al. (2000). Data points in the $170\mu m$ plot: filled circles: Dole et al. (2001), open square: Matsuhara et al. (2000), open diamonds: total counts of Juvela et al. (2000), open triangles: counts of multiple detections of Juvela et al. (2000). The SCUBA $850\mu m$ counts: crosses: Blain et al. (1999); open circles: Hughes et al. (1998); open diamonds: Eales et al. 2000; open squares: Barger et al. (1999); filled diamonds: Scott et al. (2002). The cosmic IR background: Filled circles: Lagache et al. (1998); open squares: Finkbeiner et al. (2000); open stars: Gorjian et al. (2000); filled star: Dwek and Arendt (1998); large crosses: SCUBA source count results (Blain et al. 1999); shadowed area: the range of COBE/FIRAS results (Fixsen et al. 1998); diamonds and Xs with upper-limits: upper-limits from TeV gamma-ray radiation of Mrk403 and Mrk501 (Dwek & Slavin 1994; Stanev & Franceschini 1998).

Fig. 3.— Comparisons of predictions of Model S2 with observed IR counts and CIB. The sources of data points are the same as in Fig.2.

Fig. 4.— Comparisons of predictions of Model S3 with observed IR counts and CIB. The sources of data points are the same as in Fig.2.

Fig. 5.— Predictions of Model S1 for redshift distributions of various IR surveys. The observed redshift distributions (histograms in corresponding plots) of IRAS $60\mu m$ sources and ISOCAM $15\mu m$ sources are taken from Rowan-Robinson (2001) and Franceschini et al. (2001), respectively.

Fig. 6.— Predictions of Model S2 for redshift distributions of various IR surveys. Otherwise same as in Fig.5.

Fig. 7.— Predictions of Model S3 for redshift distributions of various IR surveys. Otherwise same as in Fig.5.

Fig. 8.— Comparisons of model predictions for the $15\mu m$ luminosity functions (LFs) with observations. The data points for $z=0$ LF are taken from Xu (2000). The solid line is the Schechter function fit of the data points. Points in other panels are derived using data taken from Elbaz et al. (2002).

Fig. 9.— Star formation history (SFH) predicted by new models. Data points: Red arrows with error bars: lower limits derived from the $15\mu m$ LFs in Fig.8 (see text). Filled squares: SFR from ISOCAM surveys (Flores et al. 1999b). Xs: SFR from Balmer line surveys (Gallego et al. 1995; Tresse & Maddox 1998; Yan et al. 1999; Glazebrook et al. 1999). Open squares: SFR from UV surveys (‘extinction corrected’ data taken from Fig.9 of Steidel et al. 1999). Open triangle: SFR from SCUBA (Barger et al. 1999). The shaded area: predictions by Pei & Fall (1995). All data have been converted to the cosmology model specified by $H_0=75$ km/sec/Mpc, $\Omega_m = 0.3$, and $\Omega_\Lambda = 0.7$.

Fig. 10.— Schematic plots of formation functions of three E/S0 models.

Fig. 11.— Color v.s. redshift diagrams of E/S0 galaxies. Model predictions compared with observations (open diamonds, Franceschini et al. 1998).

Fig. 12.— Model predictions for the redshift distribution of E/S0s in HDF-N compared with the data (histogram, Franceschini et al. 1998).

Fig. 13.— Counts in the UV (2000Å), B, R and K bands. Predictions of Model S1 (for dusty galaxies) plus predictions of Model E2 (for E/S0s) are compared to data. Data points in the UV (2000Å) plot: Milliard et al. (1994). Data points in the B-band plot: Open squares: Williams et al. (1996); filled squares: Metcalfe et al. (1995); Xs: Metcalfe et al. (1991); open diamonds: Gardner et al. (1996). Data points in the R-band plot: open squares: Lin et al. (1999); open diamonds: Cohen (2002). Data points in the K-band plot: open triangles: Bershadsky et al. (1998); open squares: Soifer et al. (1994); Xs: Minezaki et al. (1998); open diamonds: Gardner et al. (1996). Data points in the $6.7\mu m$ band plot: open squares: Taniguchi et al. 1997; Xs: Altieri et al. 1999; diamond: Flores et al. 1999a; shaded area: Oliver et al. (2002) and Serjeant et al. (2000). Data points in the $12\mu m$ band plot: open squares: Fan et al. 1998; Xs: Clements et al. 1999.

Fig. 14.— Counts in the UV (2000Å), B, R and K bands. Predictions of Model S2 (for dusty galaxies) plus predictions of Model E2 (for E/S0s) are compared to data. Data points are the same as in Fig.13.

Fig. 15.— Counts in the UV (2000Å), B, R and K bands. Predictions of Model S3 (for dusty galaxies) plus predictions of Model E2 (for E/S0s) are compared to data. Data points are the same as in Fig.13.

Fig. 16.— Model predictions for counts in three SIRTf bands ($3.6\mu m$, $24\mu m$ and $70\mu m$).

Fig. 17.— Predictions of Model S1, Model S2 and Model S3 for color distributions of ISO sources. The detection limits in these bands are set to be $f_{6.7\mu m} \geq 30 \mu Jy$, $f_{15\mu m} \geq 100 \mu Jy$, $f_{90\mu m} \geq 100 mJy$, $f_{170\mu m} \geq 180 mJy$, $R \leq 24 mag$, and $K \leq 20 mag$. The observed color distributions (histograms in corresponding plots) of ISOCAM $15\mu m$ sources in the HDF-N field are derived from data taken from Cohen et al. (2000) and Hogg et al. (2000).

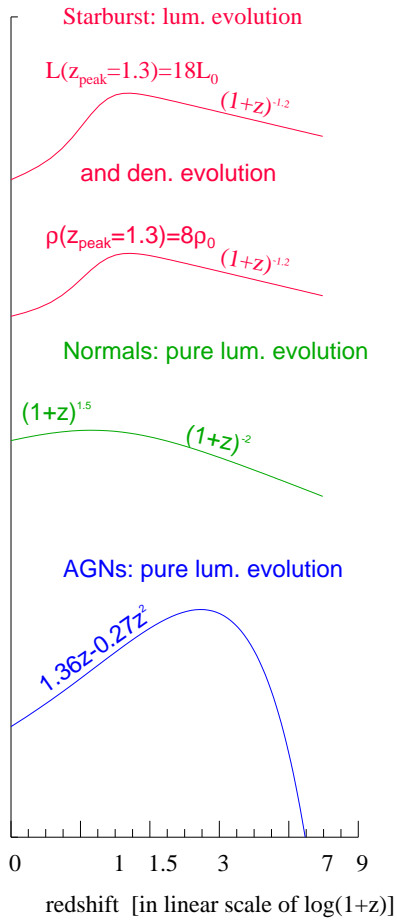
Fig. 18.— Predictions of Model S1, Model S2 and Model S3 for color distributions of SWIRE sources. The detection limits in these bands are set to be: $f_{70\mu m} \geq 6.15 mJy$, $f_{24\mu m} \geq 0.45 mJy$, $f_{3.6\mu m} \geq 7.3 \mu Jy$, $f_{8\mu m} \geq 32.5 \mu Jy$, $R \leq 25 mag$, and $K \leq 20 mag$.

Fig. 19.— Panel *a*: $25\mu m$ local luminosity functions (LLFs) of three populations of dusty galaxies. Different lines denote different assumptions on the evolution of the sources: solid line — no evolution; dashed line — $q=3.0$; dashed-dot line — $q=4.5$. Panels *b*, *c*, and *d*: Plots of pairwise covariance of the LLF parameters. The ellipses show the 68% confidence intervals. The lines are the same as in panel *a*.

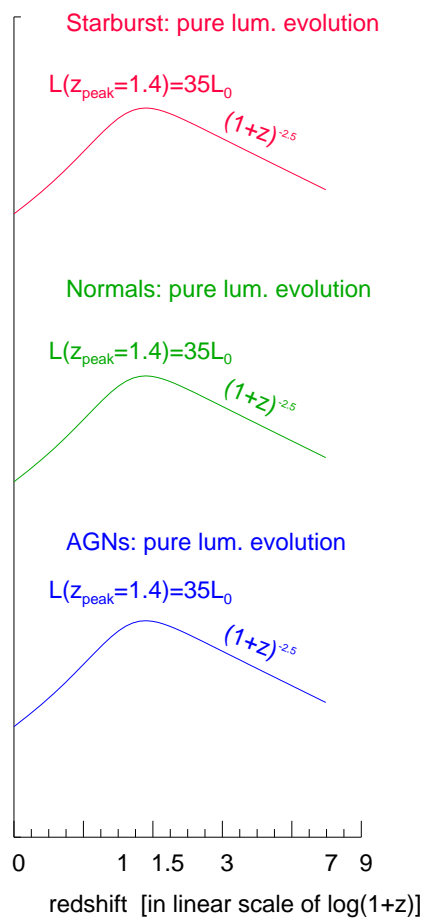
Fig. 20.— The UV-B v.s. B-K correlation of galaxies. Data for ULIRGs (large crosses) are taken from Trentham et al. (1999). Other data are taken from the UV and IRAS selected sample of Xu and Buat (1996).

Fig. 21.— The model SED of M82 compared to data. Data points: filled squares: collections of Silva et al. (1998); open squares: 2MASS and NED data.

Model S1:



Model S2:



Model S3:

